The Journal of Adhesion

ISSN: 0021-8464 (Print) 1545-5823 (Online) Journal homepage: www.tandfonline.com/journals/gadh20

Examination of film and paste adhesive behaviour under cryogenic conditions using a thick adherend shear test

Thomas Gesell , Dirk Holzhüter , Jens Kosmann , Martin Johannes Schollerer , Patrick Adrian Makiela & Christian Hühne

To cite this article: Thomas Gesell , Dirk Holzhüter , Jens Kosmann , Martin Johannes Schollerer , Patrick Adrian Makiela & Christian Hühne (25 Dec 2025): Examination of film and paste adhesive behaviour under cryogenic conditions using a thick adherend shear test, The Journal of Adhesion, DOI: 10.1080/00218464.2025.2600613

To link to this article: https://doi.org/10.1080/00218464.2025.2600613

Published online: 25 Dec 2025.

THE JOURNAL OF ADHESION
https://doi.org/10.1080/00218464.2025.2600613

Taylor & Francis
Taylor & Francis Group

Examination of film and paste adhesive behaviour under cryogenic conditions using a thick adherend shear test

Thomas Gesell, Dirk Holzhüter, Jens Kosmann, Martin Johannes Scholleren, Patrick Adrian Makiela, and Christian Hühne

Composite Design Department, Institute of Lightweight Systems, Brunswick, Germany

ABSTRACT

Carbon fibre reinforced polymers (CFRP) are key enablers for lightweight liquid hydrogen storage in aerospace applications. Adhesive bonding provides a structurally efficient and inherently leak-tight method for joining CFRP and hybrid substrates, offering clear advantages over mechanically fastened joints. While most studies focus on shear stress due to the technica difficulty of measuring strain at cryogenic temperatures, the brittle nature of epoxy adhesives under these conditions makes it crucial to establish clear shear strain limits to ensure both leak-tightness and structural performance. This study introduces a methodology for characterising structural film and paste adhesives using thick adherend shear tests under cryogenic conditions. The approach incorporates the development of a dedicated cryogenic test rig (CryoTAST) and the adaptation of a custom-built capacitive extensometer suitable for use at cryogenic temperatures. Shear properties of four adhesives were determined in accordance with ASTM D5656. Furthermore, the influence of manufacturing variability was assessed by evaluating three bondline thicknesses per adhesive. The results provide essential input data for the robust design and qualification of adhesively bonded joints in CFRP liquid hydrogen tanks, supporting both their mechanical performance and leak-tightness under extreme environmental conditions.

ARTICLE HISTORY
Received 24 July 2025
Accepted 25 November 2025

KEYWORDS
Adhesive characterisation; cryogenic applications; strain measurement; CFRP liquid hydrogen tank; aerospace

1. Introduction

Liquid hydrogen, long established as an energy carrier for upper stage rocket propulsion, is now additionally under investigation as a replacement for kerosene in commercial aviation to support decarbonisation and sustainability goals. While the structural requirements for hydrogen storage tanks differ significantly between space and aeronautical applications, both sectors are pursuing lightweight solutions, with CFRP emerging as a promising alternative to traditional

CONTACT Thomas Gesell thomas.gesell@dlr.de Composite Design Department, Institute of Lightweight Systems, Lilienthalplatz 7, Brunswick 38108, Germany

This article was originally published with errors, which have now been corrected in the online version. Please see Correction (https://doi.org/10.1080/00218464.2026.2634535)

metals for cryogenic tank construction. In this context, adhesive bonding is being explored as an enabling technology for various joint types – including segmentation joints, feedthroughs, suspension mounts, sandwich structures, insulation attachment, and system component mounts – each presenting distinct requirements for adhesive selection. Using adhesive bonding as a joining technique within a cryogenic environment is not a new idea.

The mechanical characterisation of adhesives under cryogenic conditions dates back to the 1960s and 1970s, with pioneering studies by Hertz,[1,2] Althof,[3] and Gosnell et al.[4] These early works primarily investigated lap shear strength of metallic joints, focusing less on intrinsic adhesive properties such as shear modulus or ultimate shear strain. Hertz evaluated a range of adhesives – including epoxy-based, nitrile-phenolic, and polyurethane types – using single lap shear and butt tensile tests across temperatures from room temperature down to liquid nitrogen temperatures. Notably, the epoxy-nylon adhesive "Metlbond 406" showed the highest lap shear strength at cryogenic temperatures. Althof expanded these studies by analysing several epoxy and phenolic adhesives with aluminium and stainless steel adherends, demonstrating that pure epoxy and epoxy-polyamide adhesives maintained strength even after prolonged cold storage. Gosnell et al.[4] tested several polymeric adhesive groups at LN2 condition using 7075 aluminium adherends in thin single lap shear and peel tests. Highest shear strength was achieved by a polyurethane adhesive. At the end of the 1970s, Roseland[5] and Williamson et al.[6] summed up the experience gained by NASA and subcontractors and published state-of-the-art review studies on adhesive joint behaviour at cryogenic conditions.

A resurgence of research around the millennium brought a focus on composite joints, with Goeders et al.,[7] Graf et al.,[8] Raffaelli[9] leading efforts to characterise lap shear strength and, for the first time, some tensile stress-strain behaviour of pure adhesives at cryogenic temperatures. Goeders et al.[7] investigated adhesive bonding for PEEK/IM-6 thermoplastic composites. Two adhesive systems – FM 300 and EA 9394 - were identified as highly effective across extreme temperatures from −269°C to 121°C, demonstrating reliable performance for bonding both similar thermoplastic materials and thermoplastics to titanium. Graf et al.[8] used double lap shear specimens made from IM7/977–2 composite to evaluate epoxy, polyurethane, and cyanate ester adhesives at 24°C and −253°C. Surface preparation influenced performance, with sanded surfaces performing best in cryogenic conditions and peel ply-prepared surfaces excelling at room temperature. The highest shear strength, was achieved by the "HT424 Film" epoxy-phenolic adhesive with aluminum additive. Raffaelli[9] investigated the performance of a cryogenic adhesive (EA 9361) and a high-temperature adhesive (EA 9321) by testing pure adhesive tensile specimens, single lap shear specimens, and double lap shear specimens across a temperature range from 40°C to −269°C. Notably, both systems exhibited a pronounced increase in elastic modulus from room temperature

to cryogenic conditions, as measured by strain gauges on tensile bulk specimens. Although the cryogenic adhesive was significantly more flexible at room temperature, at −196°C both adhesives displayed nearly identical elastic modulus and elongation at break. Additionally, Raffaelli attempted to derive the adhesive shear stress-strain relationship from single lap shear specimens using a strain gauge, but finite element analysis revealed that this method was unsuitable due to significant deformation of the thin adherends influencing the measured shear modulus.

More recent studies form a third wave, exemplified by Alberts et al.,[10] and Leitwein et al.[11,12] Alberts et al. analysed the mechanical behaviour of epoxy adhesives used in multilayer insulation standoffs, applying a test method oriented tailored towards practical application. In 2021 Leitwein et al. contributed by introducing the a thick adherend shear test for characterising adhesive shear stress-strain relations at cryogenic temperatures, employing a strain gauges based extensometer and finite element analysis to address measurement challenges posed by specimen deformation. Their work under the ESA ABCE2019 project advances standardised testing for adhesive joint design in cryogenic environments. Unfortunately by submission date of this study neither shear stress-strain curves nor shear modulus at cryogenic test conditions were published by Leitwein et al.

In summary, it can be concluded that most characterisation programmes which were dedicated to adhesive joint evaluation under cryogenic conditions focus on lap shear joint strength[1–4,9,13] or adhesive strength.[8,9] Some studies have explored non-standard test methods,[10,14] often inspired by specific applications, which offer only limited insight into general adhesive joint behaviour. Furthermore, studies[3,7,9] demonstrate that stable or increasing joint shear strength can be achieved at decreasing temperatures, provided that an appropriate epoxy-based adhesive is selected. However a significant increase in elastic modulus and a marked reduction in elongation at break can be expected at cryogenic conditions even for suited adhesives. Attempts to determine shear stress-strain behaviour of adhesives at cryogenic conditions based on thin single lap shear specimens were not successful.[9] A method based on TAST specimen with a single strain gauge based extensometer was proposed, but no results were published.[11] The preceding review highlights a clear gap: adhesive shear stress – shear strain behaviour, shear modulus, and shear strain at failure are not available for cryogenic conditions. Nevertheless, these are critical parameters for joint design and numerical simulation. This is particularly relevant for cryogenic applications, given the brittle nature of epoxy adhesives and the preload induced by the mismatch in the coefficient of thermal expansion (CTE) between the adhesive and the adherends. This study seeks to close this gap by presenting an alternative testing method and an adopted capacitive extensometer. The practical implementation of this method was illustrated through characterisation of four adhesives.

Furthermore, the importance of understanding the shear stress-strain behaviour for the design of joints subjected to cryogenic loading was emphasised. Finally, the influence of bondline thickness on adhesive performance was investigated.

2. Methods

For the determination of the shear stress-strain behaviour it is advisable to rely on a test standard that imposes a stress state as close as possible to pure shear stress within the overlapping area. DIN EN 14869–1[15] proposes a torsion testing method using butt-bonded hollow cylinders. However, this method requires complex strain measurements in the bondline region, even at room temperature. Due to the challenges associated with strain measurement at cryogenic temperatures, the demand for high testing rates, and the difficulties related to load introduction within the cryogenic bath, this method was not employed. The TAST-based methods described in ASTM D5656[16] and ISO 11003–2[17] provide more suitable options for cryogenic testing. These tests make use of thick adherends which suppress peeling loads on the bondline due to their bending stiffness. Furthermore, extensometers are used at the flanks of the specimen in order to measure specimen deformation within the overlapping area as close to the bondline as possible. A short overlapping length is used to approximate homogeneous shear stress within the bondline length direction, since standards only evaluate mean shear stresses within the bondline. However, the mean shear stress results derived from these standards must be interpreted in the light of Volkersen's[18] shear stress distribution formulation for a lap shear configuration showing significant stress concentration at the overlapping ends due to an abrupt change in stiffness. In contrast to joint strength evaluation, determining the shear stress – strain curve is considerably more challenging, as joint deformation within the overlap region must be measured directly in the cryogenic environment, and as close as possible to the bondline. The measured deformation comprises contributions from both the adherends and the adhesive. Due to the increased stiffness of adhesives at cryogenic temperatures,[9] the measurable adhesive deformation is significantly reduced. As the proportion of adhesive deformation within the total signal decreases, the measurement accuracy generally decreases in TAST testing.[19] Leitwein et al.[11] present a TAST specimen setup for cryogenic testing, with an extensometer mounted on the top surface of the specimen, as shown in a photograph. Contrary to the best practices described in the standards,[16,17] deformation was not measured in close proximity to the bondline at the specimen flanks. Consequently, the adhesive's contribution to the overall deformation signal is further reduced. This is particularly noteworthy, as Leitwein et al.[11] themselves correctly identified the reduced adhesive deformation fraction under cryogenic conditions as a challenge for

measurement accuracy. Based on this observation, it can be concluded that, for cryogenic testing, deformation should be measured on the specimen flanks, as close as possible to the bondline, in order to minimise measurement errors. This recommendation aligns with the findings of Kassapoglou et al.[19] regarding the characterisation of thinner bondlines in general TAST testing. Schematic drawings and setup images provided by Leitwein et al.[11] also indicate a relatively rigid clamping configuration. However, TAST specimens are particularly sensitive to misalignment, which should preferably be addressed through appropriate bearing. To detect, assess, and compensate for potential misalignment effects, at least two sensors – mounted on opposite flanks of the specimen – are required. Based on the provided photograph,[11] it appears that a single sensor strain gauge-based extensometer from SANDNER Messtechnik GmbH was used on one specimen side. From the specimen it can be assumed, that specimens were manufactured individually rather than as part of a series plate based batch production.

Taking these considerations into account ASTM D5656 was used, to examine shear stress-strain behaviour at cryogenic conditions. Development was built upon existing test and manufacturing infrastructure developed for testing close to room temperature conditions.[20] Figure 1 shows (a) the TAST specimen, (b) the overlap region where deformations under tensile load are measured using an extensometer on both specimen flanks, and (c) a schematic of the extensometer used. The extensometer engages with the specimen via pins

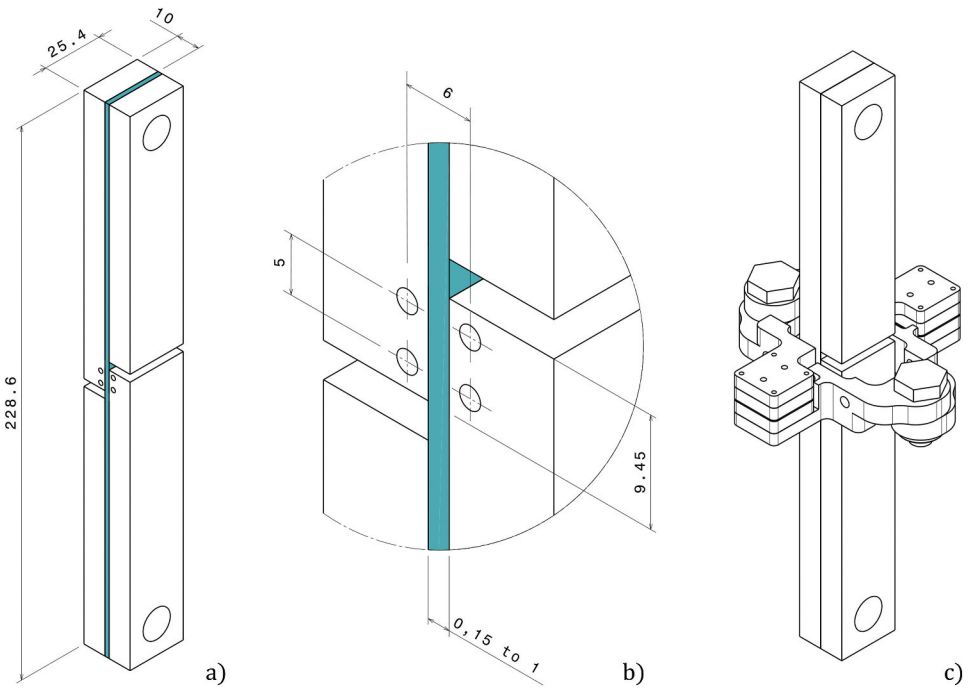

Figure 1. (a) TAST specimen; (b) Overlapping area; (c) Installed capacitive extensometer.

that fit into the holes shown in (b). The deformation of the specimen was measured close to the adhesive layer. Due to the small strains involved, the displacement signal from the testing machine would be unsuitable.

2.1. Specimen manufacturing

The quality of an adhesive joint depends heavily on the manufacturing process. Therefore, a Life Data Sheet (LDS) was created for each series, documenting the fabrication procedure. As well as precise work instructions, the LDS includes mandatory quality assurance steps that must be confirmed with a signature and timestamp. TAST specimens series were manufactured from two aluminium plates (250 × 250 mm) made of the alloy AL7075. After acclimatisation of the adherends, the process began with a flatness inspection of both joining partners. Surface pre-treatment was then performed. Plates and aluminium spacers were first degreased with acetone, followed by isopropanol. The bonding surfaces were subsequently sandblasted using corundum grit (F180). Sandblasting was performed at a system pressure of 4 bar, with the nozzle positioned at a 45° angle relative to the plate surface and a distance of 10 cm between the nozzle and the plate. Following the blasting, a visual inspection was conducted to verify a uniform surface appearance. Any residual blasting medium was removed using isopropanol. Prior to adhesive application, the environmental conditions at the bonding site were checked and documented.

For paste-like adhesive systems, aluminium spacers were placed outside the intended overlap area before applying the adhesive in an X-pattern onto plate A. Figure 2(a) illustrates this step. The area without spacers is marked in red. Subsequently, plate B was positioned on top. Curing of the aerospace adhesive systems was carried out at elevated temperatures under pressure in a hydraulic press. Cryogenic adhesive systems, on the other hand, were cured using screw clamps. Due to the extended curing times of the cryogenic adhesives at room temperature, the use of the hydraulic press was avoided to prevent unintended heating and to ensure curing under ambient conditions. Adhesive curing was

Figure 2. Steps in the TAST specimen manufacturing process: (a) Paste adhesive applied to plate a with spacers in place; (b) Outer contour milled; (c) Individual specimen bars with slots machined from the bonded plate.

performed in accordance with the manufacturer's specifications (see Subsection 2.6).

After complete curing of the bonded TAST plates, mechanical processing was carried out using a semi-automated milling program. The milling was performed with a conservative cut to ensure that the specimens were manufactured as gently as possible, avoiding any damage to the adhesive joint. Each bonded TAST plate was machined in four steps to produce seven specimens per plate, forming one series. In the first step, holes were drilled and the outer contour was reduced. In the contour milling step, the individual specimen contours were cut without the slots. In the slotting step, the specimens were engraved and the slots were milled. After slot milling, the slot depth was visually inspected – both laterally using a USB microscope and from above. In all cases, the aluminium layer of the upper plate had to be completely removed, ensuring continuous visibility of the adhesive within the slot. Milling into the lower adherend was avoided. If residual aluminium was still present above the adhesive, the slot depth was iteratively increased in 0.1 mm steps. In the final machining step, the specimens were laid on their sides and recesses for the extensometer grips were milled. Figure 2(b,c) illustrate the milling process, with (b) showing the outer contour milled from the plate and (c) depicting the individual specimens extracted from the plate.Subsequently, measurements of the specimens were carried out in the overlap region using a microscope. The overlap length and the adhesive layer within the slot areas were visually documented for each specimen. Exemplary results of the previously described slot milling process are shown in Figure 3, based on microscope images.

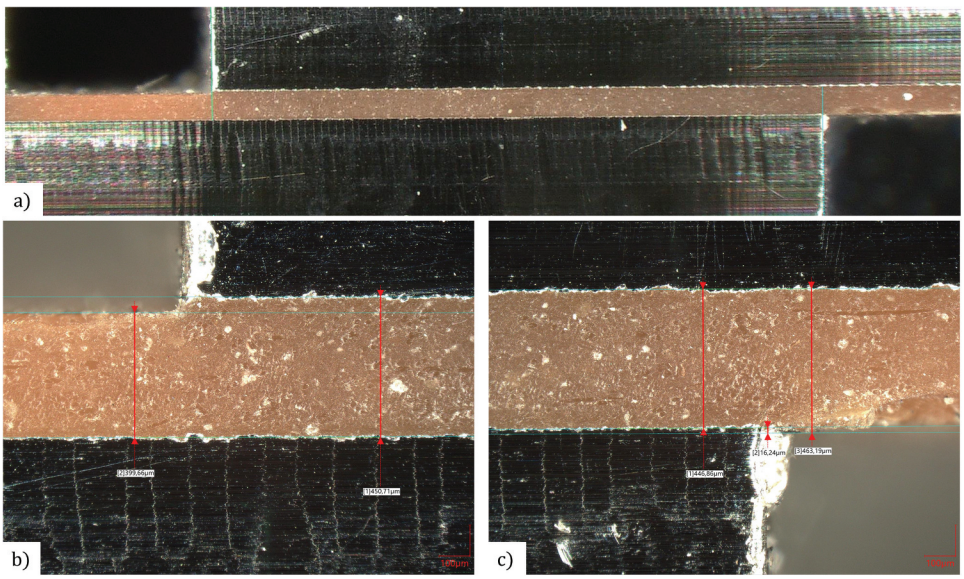

Figure 3. Specimen microscopy: (a) Overview of the overlap region; (b) Left slot; (c) Right slot.

In contrast to the plate-based serial manufacturing approach adopted in this study, Kadioglu et al.[21] propose a single-specimen method using two steel adherends and an adhesive fillet at the run-out. They identify five disadvantages of plate-based fabrication, which are reassessed here in the context of the DLR manufacturing process. The first concern raised relates to potential changes in adhesive properties caused by heat input during milling. However, due to the higher machinability of Al 7075 compared to steel, the use of a gentle material removal process, the approximately threefold higher thermal conductivity of Al 7075, and the use of ethanol as a coolant, the plate temperature during milling remains below 40 °C. Ethanol evaporates without residue and is classified as compatible with the epoxy adhesives employed. The adhesives used are industrial-grade systems also intended for the manufacturing of bonded LH2 tank structures, where comparable milling processes are conducted. The material testing therefore encompasses this condition as a potential worst-case scenario. The second concern relates to edge integrity. Microscopic inspection of all tested specimens revealed no milling-induced adhesive damage. The measured shear strengths met or exceeded manufacturer's specifications, confirming process suitability. Attention was also drawn to potential issues in slot milling by Kadioglu et al.[21] Within this work, the milling operation terminates at the adhesive layer, ensuring that the adhesive contained in the slot was not removed during machining (see Figure 3). While continuous adhesive layers can introduce minor axial stresses, the stiff adherends dominate load transfer, rendering this effect negligible in the center area of the bond (see Figure 9) where deformations are measured. Kadioglu et al.[21] also recommend modelling an adhesive fillet at the run-out region as part of the manufacturing process. Although this represents an academically ideal condition, comparable specimen-level processes at DLR using shims and an alignment jig for fibre-optic sensor integration in TAST specimens yielded inferior alignment and bondline thickness quality compared with the plate-based method. Furthermore, Kadioglu et al.[21] provide only schematic and numerical representations, without microscopic evidence verifying the fillet quality. Their adhesive thickness tolerances are comparable to those achieved for the structural adhesives in the present study. However, whereas Kadioglu et al.[21] determined the bondline thickness indirectly, this work performed direct microscopic measurements at three positions within the overlap region for each tested specimen. In addition, the present programme investigated thinner adhesive layers (down to 0.15 mm) and included both paste and film adhesive systems, which required adaptable manufacturing processes to ensure consistency. The potential impact of plate flatness on bondline quality was also highlighted as a concern by Kadioglu et al.[21] Therefore, cast and precision-milled Al 7075 plates were used for specimen manufacturing in this study. Measured bondline variations are consistent with those reported by Kadioglu et al.[21] for structural adhesives. Finally, specimen reuse, considered

an advantage of single-specimen manufacturing by Kadioglu et al.,[21] was not an objective in this study. As film adhesives cannot be removed without altering specimen dimensions, reusability was deemed irrelevant. Overall, the plate-based manufacturing route used in this study constitutes a robust and repeatable alternative to the single-specimen fabrication method of Kadioglu et al.[21]

2.2. TAST and CryoTAST setup

The DLR-TAST test rig illustrated in Figure 4 was developed by Kosmann et al.[20] for common aeronautical temperature conditions ranging from −55°C to 80°C. Temperature conditions were applied via a climate chamber. The DLR-TAST test setup was installed in a universal testing machine used to apply mechanical tensile load. It consisted of load-introducing structures that allowed proper self-alignment of the specimen during the test by using ball joints and bushings. Force was measured via universal testing machine load cell while deformation in the overlapping area was measured by an extensometer consisting of two capacitive displacement sensors facing towards individual targets. For room temperature testing, CSH2FL-CRm1.4 capacitive displacement sensors manufactured by Micro-Epsilon were used. Additionally, the measurement chain included a DL6220 demodulator and a DT6220 multi-channel capacitive system. Targets and sensors Were mounted on two separate rigid aluminium clamping fixtures, which were clamped independently onto the specimen halves. After specimen failure

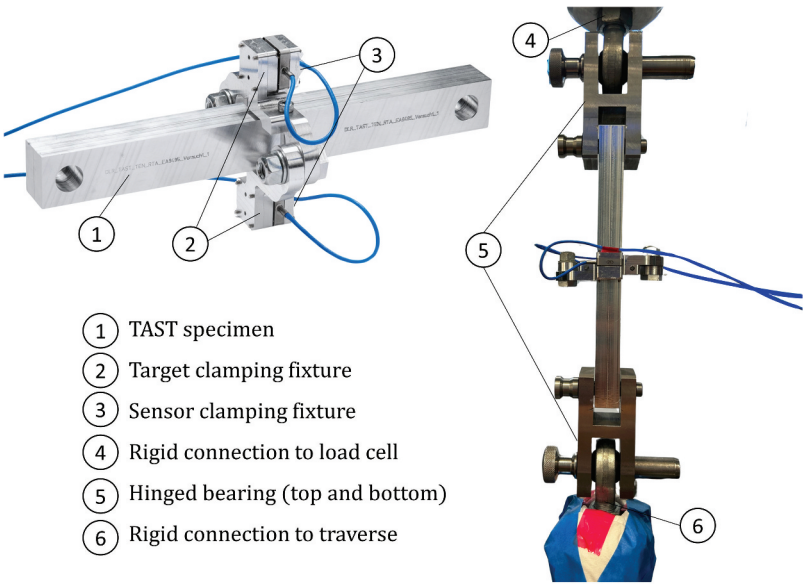

Figure 4. Room temperature TAST setup.

target clamping fixture remained mounted on the lower half, while sensor clamping fixture remained mounted on the upper specimen half. The distance change between capacitive displacement sensors and their corresponding targets imposed by mechanical loading was used to calculate shear strain. For the reproducible positioning of the sensor, bore holes were milled out of the specimen flanks close to the overlapping area of the bondline (see Figure 1(b)). Each clamping fixture engaged with two pins per side in the corresponding holes in the the specimen flanks. Pretension was applied via screw connections for each separate clamping fixture in order to fixate it on the later specimen halves within the boreholes by pins (see Figure 1(c)).

Based on DLR-TAST setup the DLR-CryoTAST setup illustrated in Figure 5 was developed for cryogenic testing. Cryogenic temperature conditions of −196°C were applied within the overlapping region of the specimen by liquid nitrogen. The cryogenic fluid was contained within a foam-isolated reservoir that encloses the specimen, extensometer and parts of the load-bearing structure. Following the philosophy of Kosmann et al.[20] ball joints and bushings were used for a proper self-alignment of the specimen during the test. Considering CTE mismatches during cryogenic testing, plain bearing and shaft tolerances were adapted in order to equal the tolerances of the room temperature test rig during room temperature testing to allow for proper alignment. In the initial design, a continuous heat conduction path through the load-bearing structure at the bottom of the container presented a major challenge. Rising nitrogen gas bubbles, caused by parasitic heat input,

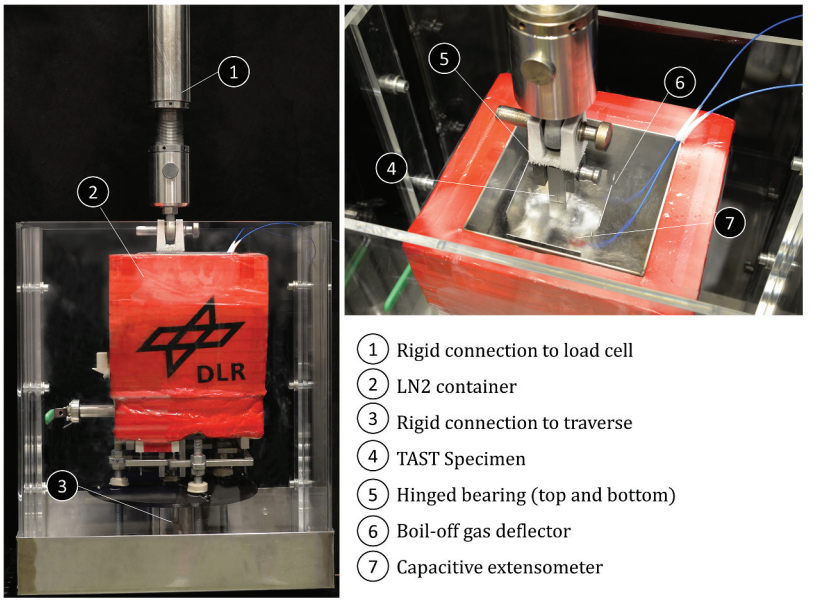

Figure 5. Cryogenic temperature CryoTAST setup.

interfered with the extensometer signal and affected measurement accuracy. The problem was mitigated by a second design that relied on a separation of the metallic heat conduction path via several pressure-loaded ceramic components. Usually glass fibre reinforced polymers (GFRP) are used for this kind of problems and would result in better insulation performance. However, GFRP was not used in this case to ensure a rigid load path and avoid settling displacement during the tensile test. Cermaic elements within the load path were preloaded by 20 kN during assembly while testing was conducted below 16 kN. CSH2FL(20)-CRm1.4 capacitive displacement sensors were employed for cryogenic testing. Target spacers were adapted to reduce the distances between the targets and the sensors. The same rigid aluminium clamp concept was used as described for the room temperature testing. Below the extensometer a boil-off gas deflector was installed to reduce signal disturbance via gaseous nitrogen bubbles.

2.3. Experimental procedure – CryoTAST

The test procedure began with mounting the target and sensor clamping fixtures onto the specimen, followed by installing the instrumented specimen into the test setup. A preliminary tensile load of approximately 300 N was then manually applied to seat the assembly, ensure proper alignment, and eliminate slack. Subsequently, force control mode Was activated to maintain a constant load. Liquid nitrogen (LN2) was slowly introduced into the container, while force control compensated for thermal contraction of the assembly via traverse movement. Load fluctuations remained below 50 N. The LN2 level Was raised well above the schematic representation in Figure 5, immersing the specimen fully into the cryogenic fluid, which required approximately 4 L of LN2. This filling process constituted a thermal shock for the joint, yielding conservative test results. This extreme scenario would be avoided in actual cryogenic composite tank applications. Thermal strains in the region of the extensometer induce variations in the absolute distance between sensor and targets, particularly under transient conditions such as cooling or heating. Therefore, prior to the application of any mechanical load, each specimen undergoes a cooling phase of 10 minutes to ensure that the overlap region is fully equilibrated at the target temperature of −196°C. The required cooling duration was determined through numerical thermal simulations and validated experimentally using fibre-optic sensors embedded within the adhesive layer. During this preloading cooling phase, the absolute distance between sensor and targets changes due to thermal contraction of the specimen. Once cooling is complete, a reference state is established. A preload of 500 N was then automatically applied to ensure a consistent starting position, the extensometer signal was zeroed and data acquisition was initiated. During the mechanical loading, both the specimen and the extensometer remain thermally stable, so no additional

thermal deformation occurs. Consequently, any measured changes in distance during the test are solely attributable to the applied mechanical load. The traverse proceeded at a constant rate until specimen failure, with the load applied in position-controlled mode. The test speed was set to 0.05 inch/min for both room temperature (RT) and cryogenic temperature (CT) conditions. After the test, approximately 3 L of LN2 were drained, leaving about 1 L in the container. The lower bolt was removed using tongs while still submerged in LN2 to prevent bearing freezing and to compensate for thermal expansion. The extensometer remained untouched for ten minutes after draining, as previous tests hadhave shown that abrupt handling may damage the sensors. Finally, the specimen halves and extensometer components were removed and reheated in an oven, while the next specimen is prepared using a second cryogenic extensometer. This procedure enabled the testing of approximately six specimens per day under cryogenic conditions, compared to around fifteen specimens per day at room temperature.

2.4. Strain measurement in liquid nitrogen

In order to achieve cryogenic test temperatures within the overlap region of the adhesive joint, both the specimen and the strain measurement system were immersed in a liquid nitrogen bath. The cryogenic temperature itself, as well as the physical presence of boiling liquid nitrogen, introduce parasitic effects that affect the measurement accuracy of any instrumentation used under such conditions. No off-the-shelf extensometer or alternative strain measurement system was available which was specifically designed for ASTM D5656 under such conditions. Consequently, no adequate manufacturer-certified calibration protocol existed for such measurements. Thus, comparable publications typically reported only shear strengths, while omitting measurements of shear strain at failure or shear stiffness. Within the scope of this work, a novel approach based on capacitive displacement measurement is proposed. This subsection presents the physical principles governing the operation of the measurement system under the aforementioned conditions and describes the experimental determination of a linear correlation between the voltage signal and the deformation of the adhesive layer in the CryoTAST test rig. This experimentally derived correlation forms the basis for the operation of the capacitive extensometer developed at DLR.

Capacitive displacement sensors operate based on the principle of a parallel-plate capacitor, where the capacitance C depends inversely on the instantaneous plate separation d according to

$$C = \varepsilon_0 \varepsilon_r \frac{A}{d}, \tag{1}$$

with ε_0 denoting the vacuum permittivity, ε_r the relative permittivity of the dielectric medium between the plates, and A the electrode area. To perform displacement measurement, an alternating current (AC) excitation of known amplitude I_0 and angular frequency ω is applied to the capacitor:

$$I = I_0 \sin(\omega t), \tag{2}$$

The charge Q on a capacitor is given by the integral of the current I over time

$$Q = \int I\,dt = \int I_0 \sin(\omega t)\,dt$$

$$= -\frac{I_0}{\omega}\cos(\omega t) + K \tag{3}$$

where K is the integration constant determined by the initial conditions. The correlation between current U charge Q and capacitance C is defined by

$$U = \frac{Q}{C} \tag{4}$$

Inserting formulas (1) and (3) into formula (4) yields the following expression. This expression corresponds to the simplified equation given by Bressler et al.[22] for a plate capacitor loaded by the alternating current defined in Equation (2).

$$U = \frac{-\frac{I_0}{\omega}\cos(\omega t) + K}{\varepsilon_0 \varepsilon_r \frac{A}{d}}$$

$$= -\underbrace{\frac{I_0 d}{\omega \varepsilon_0 \varepsilon_r A}}_{U_0}\cos(\omega t) + \frac{Kd}{\varepsilon_0 \varepsilon_r A} \tag{5}$$

The demodulator processes the U signal and extracts its amplitude U_0. Thus the demodulator outputs a slowly varying analogue signal which is easier to process. By demodulating, the high-frequency carrier (the original AC signal) is removed, leaving only the information that changes with the distance of target and sensor. Following this, if a constant alternating current I flows through the capacitive sensor, the amplitude U_0 of the alternating voltage on the sensor is proportional to the distance d between the capacitive sensor and target. The relation can be described as

$$U_0 = \frac{I_0}{\omega \varepsilon_0 \varepsilon_r A} \cdot d \tag{6}$$

At For room temperature condition and with air as dielectric medium $\varepsilon_r = \varepsilon_{air} = 1.0006$ can be assumed. For this condition a calibration protocol

was provided by the sensor manufacturerr, which includes the linear correlation of U_0 and d_{air} (Equation 7) as well as linear deviation for the measurement chain.

$$d_{air} = 0.4\frac{\mu\mathrm{m}}{mV} \cdot U_0 \tag{7}$$

Under cryogenic test conditions, liquid nitrogen serves as the dielectric medium. Unfortunately, the sensor manufacturer did not provide a test-based linear relationship for the measurement chain under these conditions. However, the manufacturer recommended a simplification: multiplying the linear correlation provided for room temperature and air by the relative permittivity of liquid nitrogen. Following this guidance, Equation 6 may be simplified as follows:

$$d_{LN2} \approx \varepsilon_{LN2} \cdot \frac{\omega\varepsilon_0\varepsilon_{air}A}{I_O} \cdot U_0$$

$$\approx \varepsilon_{LN2} \cdot 0.4\frac{\mu\mathrm{m}}{mV} \cdot U_0 \tag{8}$$

It should be noted that this simplification neglects changes in frequency (ω), current amplitude (I_O), and area (A) when transitioning from room temperature to cryogenic conditions. Moreover, it assumes that $\varepsilon_{\mathrm{air}} = 1$. Furthermore, as can be seen in Table 1, $\varepsilon_{\mathrm{LN2}}$ is frequency dependent. However, no literature values of $\varepsilon_{\mathrm{LN2}}$ at the operational frequency of the sensor were available. In the absence of a calibration protocol supporting these assumptions, the linear correlation between U_0 and d_{LN2}, as well as the associated linear deviation, were determined experimentally for the configuration employed, rather than relying on the manufacturer's simplification. The experiment accounted for the influence of liquid nitrogen at −196°C, which serves as the dielectric medium between the target and the sensor, as well as effects associated with the measurement chain. Additional factors, such as variations in the area A, were also addressed for the extensometer used.

For the acquisition of the linear correlation, a modified TAST specimen was fabricated. The modified TAST specimen designed for this purpose consists of a conventional TAST specimen, which was preliminary fractured into an upper and a lower half as illustrated in Figure 6(a). Bore holes were precisely

Table 1. Relative permittivity of LN2 for distinct frequency ranges.

$\varepsilon_{LN2}[-]$	valid for ω	reference
1.440	18 − 26 GHz	Reesor[23]
1.427	15 GHz	Smith[24]
1.538 ± 0.025	0.5 − 10.4 GHz	Hosking[25]
(1.525)	31.25 kHz	plausibilty check own experiment

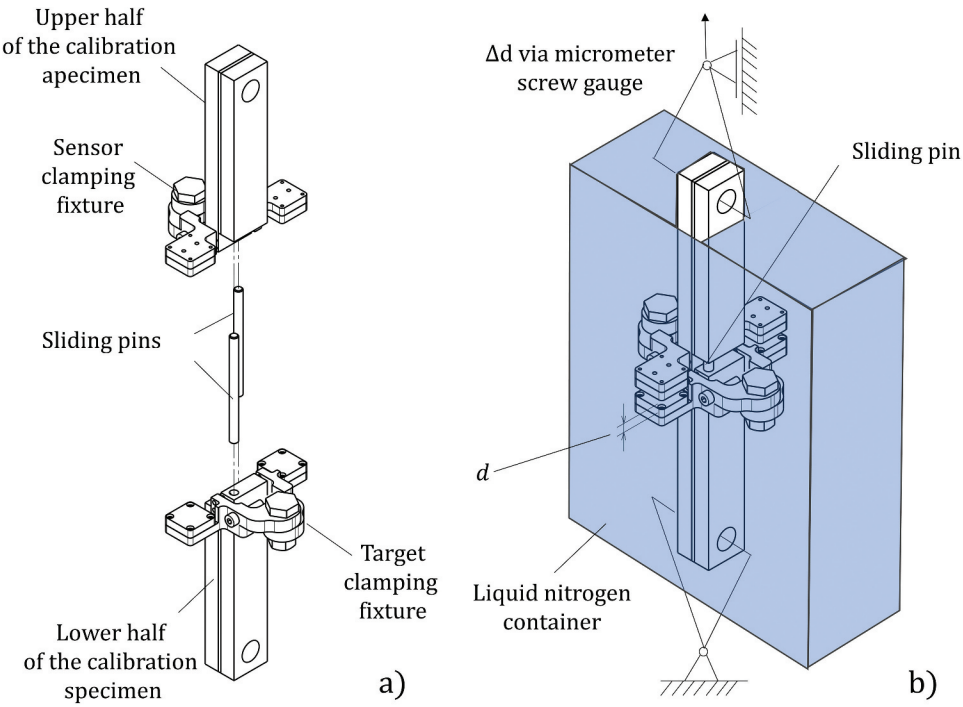

Figure 6. Experimental setup for determining the linear relationship between U_0 and d a) modiefied TAST specimen b) schematic experimental setup illustration.

machined into the specimen halves, perpendicular to the opposing faces of the aluminium adherends. Two sliding pins were inserted into the bore holes. Bore holes and sliding pin formed a clearance fit at cryogenic conditions, allowing for an axial sliding of the halves, if an axial deformation was applied. Sensor clamping fixture was mounted to the upper half, while target clamping fixture was mounted to the lower half. Figure 6(b) illustrates the schematic experimental setup in liquid nitrogen. Lower specimen half was connected to a fixed support, while upper specimen half was connected to a floating support allowing for deformation in axial direction of the specimen. A defined axial deformation was applied via a micrometer screw gauge specially designed for this purpose.

After the setup was fully cooled trough the micrometer screw gague was used to change the distance between sensors and targets in steps of 20μm, along the overall measuring range of the micrometer screw gauge (1000μm). During this process U_0 Was measured, using the described measuring chain. For each measuring step micrometers screw gauge was holed constant for 10 seconds before the next 20μm step was conducted, in order to reduce errors. Thus plateaus formed within the measured current signal. The current change between two adjacent plateaus was then correlated with a distance change

between sensor and target of 20 μm, applied via micrometer screw gauge. Figure 7 shows the calculated mean values of this current plateaus correlated with the distance change between sensor and target due to the micrometer screw gauge within a measuring range of 550 μm, which was most relevant for the adhesive characterisation.

Data were neither filtered nor smoothed. A linear regression was conducted an plotted in Figure 7 together with the linearity deviation. Using the slope of the linear function from Figure 7 and Equation 6, the following correlation between U_0 and d for testing in liquid nitrogen can be concluded, for the used measurement chain.

$$d_{LN2} = 0.60981 \frac{\mu m}{mV} \cdot U_0 \tag{9}$$

In order to asses plausibility, ε_{LN2} was calculated based on the measured linear correlation (Equation 9) of U_0 and d as well as the simplified Equation 8 given by the sensor manufacturer and listed in Table 1. Since it Was seen as a result from plausibility check including simplifications and not as a result from dedicated material characterisation, it Was given in brackets. The determined linear correlation Was considered to be plausible since ε_{LN2} calculated based on the experiment data was within the range given by Hosking et al.[25] valid for down to 500 kHz, which is at least in a close proximity to sensor operation frequency of 31.25 kHz.

It is important to understand that the extensometer signal was zeroed after cooling down and before the application of the mechanical load (see sub

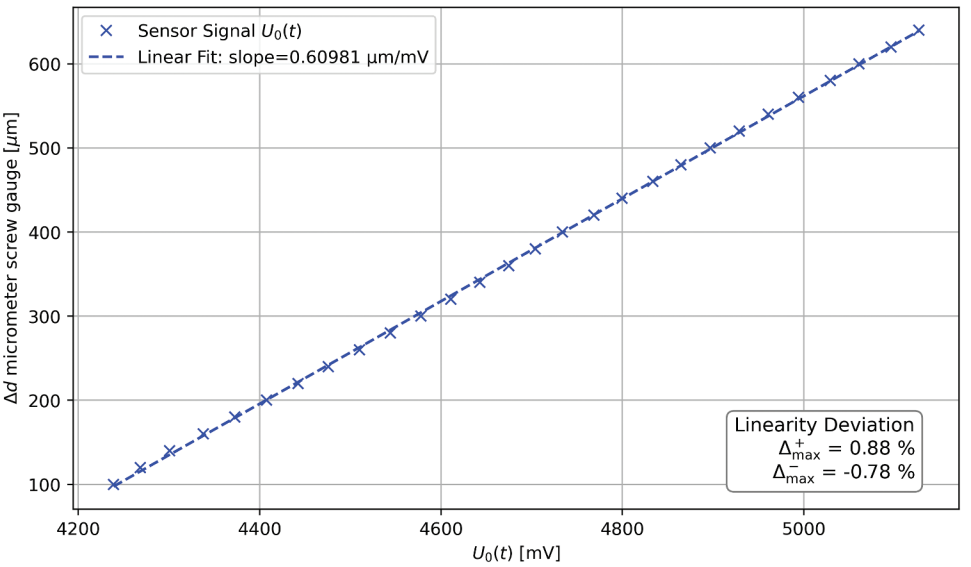

Figure 7. Plotted linear correlation of U_0 and d micrometer screw gauge for described test setup and measurement chain.

section 2.3). Thus, strains were measured based on the change in distance between targets and sensors, rather than on the absolute sensor-to-target distance. It should be noted that, in TAST tests conducted at both room and cryogenic temperatures, the extensometer captures only mechanical strains. Thermal strains occurring during transient phenomena such as cooling down are not recorded. Accurate assessment of thermal strains falls outside the scope of the TAST tests and requires dedicated experiments using alternative measurement techniques, such as thermo-mechanical analysis (TMA).

Alongside the chosen capacitive approach, alternative measurement concepts were investigated during preliminary tests. These included fibre-optic sensors (Luna ODiSI 6000) and the a strain-gauge-based extensometer (Epsilon 3442AVG) self adapted for the TAST specimen. However, neither approach was selected for the subsequent series testing. During the pre-tests, fibre-optic sensors were both embedded within the adhesive bondline and adhesively bonded to the specimen flanks. The results obtained provided valuable insight into the evolution of temperature gradients during specimen cool down. Nevertheless, several factors led to the exclusion of the fibre-optic approach for the series testing: the lack of quantified thermo-optic effects under cryogenic conditions, the complexity of the manufacturing process, concerns regarding reproducibility, and the influence of the optical fibre itself, which acted either as an obstacle within the bondline or as a potential load-bearing element when attached to the specimen flanks. The use of the strain-gauge-based extensometer proved unsuccessful due to limitations of the adapted clamping mechanism, which had to allow measurements in close proximity to the overlap region while maintaining robustness and reproducibility during testing.

2.5. Data analysis

Based on the individual linear correlation of U_0 and d elaborated in the proceeding section, deformations within the overlapping area were measured under tensile loading of the specimen at room temperature and cryogenic conditions. For both test conditions, deformation was measured independently on the opposing flanks of the TAST specimens.

Data was not filtered or smoothed, but certain characteristic events were deleted manually from the data. Three characteristic events were known to disturb the signal. At the beginning of the test, the load constant mode was active, both at room and cryogenic test conditions the activity of crosshead displacement control was visible in the sensor data for less than 1 second. Also sensor signals after specimen failure were deleted since sensor signals were not usable if sensor measurement range was exceeded after specimen separation in two halves. Despite several constructive measures, the intrusion of gaseous nitrogen bubbles into the interspace between the sensor and the target could

not be completely prevented under cryogenic conditions. These disturbed the measurement due to a change in dielectric medium from liquid nitrogen to a mixture of liquid and gaseous nitrogen for a short time. Thus relative permittivity in Equation 6 changed and the sensor signal was disturbed. These events were characterised by a short occurrence in only one of two sensor signals at a time as well as by a return to the signal, previous to the bubble event. These events were also deleted out of the data. Due to the short duration of the disturbance and the linear behaviour of the shear stress – shear strain curve under cryogenic conditions, these isolated bubble events were considered acceptable. As a distinction, fragmented failure of the bondline was visible in both sensor signals at the same time, the force-traverse displacement curve and can be acoustically witnessed.

Sensor signals from both specimen flanks were averaged to determine the overall deformation of the overlapping area. However, it is important to note, that the measured deformation was composed of adhesive and adherend deformation. Figure 1(b) illustrates the overlapping area where deformation was measured on TAST specimen. Independent of bondline thickness, the distance between bore holes where, sensor and target clamping fixture mechanically engage with the specimen was always 6 mm. Thus for thinner bondlines the portion of adhesive deformation within the overall measured deformation became less pronounced than for thicker bondlines. This lead to reduced measurement accuracy in strain detection for thinner adhesive layers. The same effect occurred during cryogenic testing, since adhesive deformation was strongly reduced due to a significant stiffness increase. In accordance with ASTM D5656[16] the deformation of the Al 7075 adherends was determined experimentally for room temperature and cryogenic conditions. For this reason aluminium reference specimens shaped like TAST specimens were milled out of solid aluminium plates and tested with the TAST and CryoTAST assembly, respectively. Following ASTM D5656[16] the adherend compliance under shear stress state (m) at 4464 N were determined based on six tests for cryogenic and room temperature. The results, are listed in Table 2. Note that m is not the reciprocal of adherend elastic modulus derived from pure tensile testing.

The determined values m_{RT} and m_{CT} were used to calculate the portion of adherend deformation d_m based on,

Table 2. Adherend compliances under shear loading (m) at a load of 4464 n, determined at room temperature and under cryogenic conditions.

m_{RT}	$8.6460 \cdot 10^{-7} \pm 3.9049 \cdot 10^{-9} \left[\frac{mm}{N}\right]$
m_{CT}	$7.8005 \cdot 10^{-7} \pm 5.8074 \cdot 10^{-9} \left[\frac{mm}{N}\right]$

$$d_m = \frac{p-b}{p} \cdot m \cdot F \tag{10}$$

where $p = 6$ mm was the distance between the bore holes where sensor and target clamping fixtures engaged, b was the measured mean bondline thickness of the individual TAST specimen in the overlapping area and F was the force measured by the load cell during the test. Adherend deformation d_m was then used as a function of F to eliminate the adherend deformation in the measured signal d and thus to calculate a corrected shear strain (γ) which represented the deformation of the adhesive portion:

$$\gamma = \frac{d - d_m}{b} \tag{11}$$

The average shear stress in the bond (τ) at each of the corrected shear strains (γ) was calculated as a function of force (F) by

$$\tau = \frac{F}{l \times w} \tag{12}$$

The overlapping length (l) was measured for each individual specimen, while the overlapping width (w) was assumed to be constant atconstantly 25.4 mm. The shear modulus (G) was calculated within the linear region by means of the secant slope based on change in shear stress divided by change in corrected shear strain.

$$G = \frac{\tau_2 - \tau_1}{\gamma_2 - \gamma_1} \tag{13}$$

Since ASTM D5656[16] does not offer a defined linear range for the determination of G, the strain values used for the tensile secant modulus were transferred from ISO 527–1.[26] Thus τ_1 was the shear stress at a corrected shear strain $\gamma_1 = 0.0005$ and τ_2 was the shear stress at a corrected shear strain $\gamma_2 = 0.0025$.

Typical shear stress-shear strain correlations for a structural adhesive are plotted in Figure 8 for a) room temperature and b) cryogenic conditions. Plots include the linear limit (*LL*) and ultimate load (*UL*) points. While the ultimate load points was characterised by specimen failure in both cases, at room temperature *LL* was characterised by a deviation from the linear region by 5% while the linear limit at cryogenic conditions was defined as the first failure of a bondline fragment. Knee point (*KN*) which which indicates the beginning of a dominate plastic yielding of the adhesive was not included in this study due to the absence of plastic deformation at cryogenic conditions.

A characteristic stepwise failure pattern was observed for structural adhesives under cryogenic test conditions (see Figure 8(b)). A potential compliance or settling behaviour of the test setup was excluded based on reference tests using

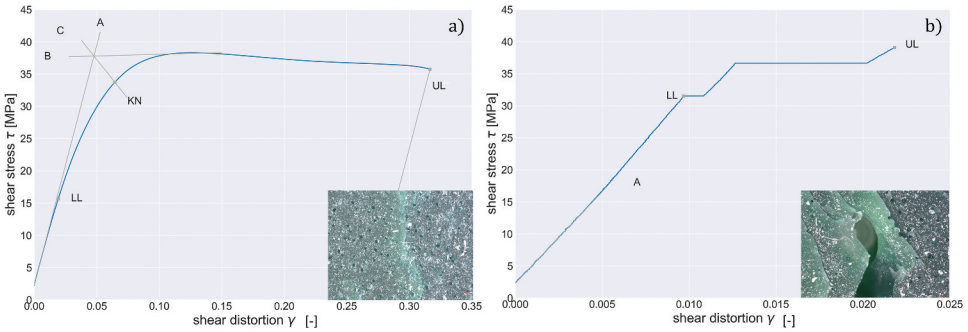

Figure 8. Example of characteristic adhesive parameters for testing at cryogenic conditions and room temperature.

rigid aluminium specimens within the relevant test range. Furthermore, stepwise failures were acoustically detectable. Microscopic analysis of the tested specimens also indicated bondline fragmentation under cryogenic conditions.

2.6. Test program

Within this study, two structural and two functional adhesives were characterised. Nominal bondline thicknesses of 0.2 mm, 0.5 mm, and 1 mm were investigated for paste adhesives, while 0.15 mm, 0.45 mm, and 0.9 mm were analysed for the film adhesive. Tests were performed at a constant temperature of −196°C in liquid nitrogen and at room temperature. For each test configuration, a series of seven specimens was manufactured and tested at DLR, resulting in a total of 168 specimens. The following adhesives were investigated:

Aeropaste 1006 is a two-component epoxy structural paste adhesive suitable for out-of-autoclave curing. It compensates for manufacturing tolerances in adhesive layer thickness and is investigated at DLR for highly loaded joints, such as CFRP segmentation joints in liquid hydrogen tanks. Series plates were cured in a hydraulic press at 0.34 bar and 93°C for 120 minutes, with temperature ramps of ± 1°C/min starting and ending at 50°C.

FM 209-1 M is an epoxy-based film adhesive with a mat carrier, also supporting out-of-autoclave curing. While less able to compensate for thickness tolerances, it generally exhibits higher strength due to fewer imperfections. It is under investigation at DLR for structural joints, such as CFRP segments in hydrogen tanks and sandwich concepts. Prior to curing, bonded plates were evacuated for one hour. Curing took place under vacuum (< 50 mbar) and hydraulic pressure (0.95 bar) at 121°C for 90 minutes, with temperature ramps of ± 1.7°C/min.

Cryobond 620N is a functional two-component paste epoxy system curing at room temperature. Thanks to its low viscosity, it wets surfaces and

penetrates leak paths, making it suitable for vacuum sealing leaking welded joints in cryogenic industries. At DLR, it is being investigated for repairing composite structures with established crack networks. Part A was liquefied at 40°C, cooled to 30°C, then mixed with Part B using a speed mixer for 2 minutes at 2000 rpm. The mixture, with a pot life of 20 minutes, was degassed in a desiccator for 4 minutes at 20–200 mbar. Curing was carried out at room temperature with four screw clamps for 24 hours, followed by six days at rest without clamping. Full cure was achieved after 7 days.

Cryobond 621 is a functional two-component paste epoxy containing 70% aluminium filler by weight, reducing CTE and increasing thermal conductivity, toughness, and modulus. Used in the cryogenic industry to reduce temperature gradients and mitigate CTE mismatch in hybrid joints, it is under investigation at DLR for hybrid joints in suspension regions. Parts A and B were preheated separately at 60°C for one hour, homogenised, cooled below 30°C, then mixed for 2 minutes at 2000 rpm. The mixture had a 60-minute pot life and was degassed in a desiccator for 4 minutes at 20–200 mbar. Curing was at room temperature with four screw clamps for 24 hours, followed by 3 days at rest; full cure was reached after 4 days.

Before testing, the overlap area of each specimen was measured. Adhesive layer thickness was determined as the average of three measurements along the overlap of each specimen. Overlap length was measured once per specimen. All measurements were performed using a microscope. Testing took place at the DLR static test lab in Brunswick, with room temperature ranging from 20°C to 27°C and relative humidity from 38% to 59%. Specimens were acclimatised in the test lab one week prior to testing.

2.7. Test simulation

During CryoTAST testing, the adhesive joint is subjected to mechanical loads that are superimposed by thermal loads induced by the cryogenic conditions. Thermal loading arises from the mismatch in coefficients of thermal expansion between the adhesive and the adherends. This mismatch induces significant pre-stress in the adhesive during cooling. To quantify this phenomenon, a simple linear elastic finite element analysis was conducted. A TAST specimen with an Aeropaste 1006 bondline thickness of 0.5 mm was modelled in Abaqus cae 2021 using C3D8R elements for both the adhesive and the adherends. All components were modelled as individual parts and merged to a single part afterwards. The mechanical material parameters used are listed in Table 4. Note that, due to the lack of material data under cryogenic conditions, calculated and assumed properties are marked with [c] and [a], respectively. Shear properties of the adhesive were obtained from the present study, while the CTE of the adhesive and adherends were measured as a function of

temperature using in-house TMA down to −150° C. In Abaqus, the CTE must be defined as secant CTE. The corresponding temperaturedependent secant CTEs for both the adhesive and the adherends are provided in Table 3. A uniform mesh size of 1 mm was applied, with a refined mesh in the adhesive region consisting of five elements across the bondline thickness to minimize edge effects in the transition zone between adhesive and adherend during post-processing. The simulation was performed using Abaqus/Standard with an implicit solver. As a simplified assumption, a homogeneous linear cooling from 20°C to −196°C was applied via a predefined temperature field. No mechanical boundary conditions were applied during the cooling step to allow thermal strains to develop freely, as in the experiment. After reaching the target cryogenic temperature, a displacement-controlled loading step was applied by prescribing a velocity of 0.25 mm/s in the bondline direction on one side of the specimen. All other translational and rotational degrees of freedom were constrained. Within the clamping region, all degrees of freedom were fully restricted to represent the experimental fixture conditions.

The simulation model and the stress distribution for a single adhesive element located at the centre of the bondline are illustrated in Figure 9. An element from the middle of the bondline was selected to quantify the influence of the combined thermal and mechanical stresses in a region representative of the average shear stress state measured with the extensometer. It should be noted that, in TAST tests, failure typically initiates due to stress concentrations within the adhesive bond at the ends of the adherends in the overlap region. However, such effects cannot be adequately captured by the simplified simulation approach or the currently available set of material parameters and are therefore addressed in a separate study.

Table 3. mechanical material parameters for simulation of Al7075 (al) and Aeropaste1006 (ad) at different temperatures ([c] calculation, [a] assumption).

Parameter	RT at 20°C	CT at −196°C	Reference
E_{Al} [Gpa]	70	85	RT,[27] CT[27]
ν_{Al} [-]	0.33	0.33	RT,[27] CT [a]
E_{Ad} [Gpa]	2	5.8	RT [c], CT [c]
ν_{Ad} [-]	0.33	0.33	RT,[28] CT [a]

Table 4. Secant CTEs for simulation of Al7075 (al) and Aeropaste1006 (ad) at different temperatures.

Temperature	α_{Al} [1/K]	α_{Ad} [1/K]
20°C	$2.00 * 10^{-5}$	$7.00 * 10^{-5}$
0°C	$2.06 * 10^{-5}$	$6.99 * 10^{-5}$
−50°C	$2.21 * 10^{-5}$	$7.19 * 10^{-5}$
−100°C	$2.13 * 10^{-5}$	$6.69 * 10^{-5}$
−150°C	$1.99 * 10^{-5}$	$5.95 * 10^{-5}$

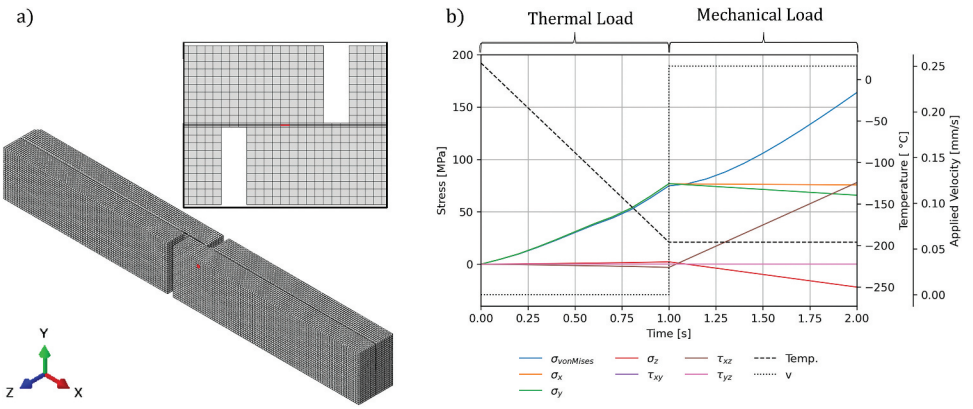

Figure 9. Linear elsatic TAST test simulation a) model and highlighted element for stress analysis b) element stress plot.

In Figure 9(b) first the thermal loading step and then the supperpostion of the mechanical stress starting at 1.0 sec can bee seen. Based on TMA data it can be assumed that cooling from room temperature to −196°C results in large thermal strains: considering free thermal deformation, approximately 11, 000 microstrain for epoxy resins, 4, 000 microstrain for the aluminium alloy. Within the adherend – adhesive system, the significantly stiffer aluminium adherends constrain the adhesive, preventing free deformation along the bondline in both the length and width directions. During cooling, the difference between the adhesive's free thermal strain and the strain of the adherend – adhesive system is responsible for the development of tensile stresses in the adhesive along the bondline length (X-) and width (Y-) directions. In the bondline thickness direction, there is no CTE mismatch, allowing the adhesive to deform freely, thus thermal normal stresses in thickness Z-direction are negliable druing the cool down phase. Same applies for the shear stresses τ_{xz},τ_{xy},τ_{yz} in the thermal load step compared to the tensile stresses σ_x and σ_y. During mechanical loading phase, as expected from the TAST experiments, the primary accumulating stress component within the adhesive is the shear stress τ_{xz}, which starts at a slightly negative value due to thermal preloading. Although the adhesive shows only minor normal stress variations in the σ_x direction during mechanical loading, a reduction in the σ_y direction can be observed, indicating the influence of lateral contraction under shear loading. In the σ_z direction, a small additional compressive stress occurs. As a simplified measure of the adhesive's strength utilisation, the von Mises equivalent stress is plotted. It becomes evident that, proceeding from the thermal to the mechanical loading phase, the overall loading of the adhesive continuously increases. The continuous rising von Mises stresses indicate that the slight stress relief in the σ_y direction caused by mechanical loading and the slightly negative shear stress τ_{xz} due to thermal preloading is of minor

relevance for the overall adhesive loading. As shown in Figure 9b), the FE analysis reveals that thermal preloading of the adhesive reduces its bearable shear load. Consequently, conservative characteristic material values are obtained within this study. The simplified linear analysis presented here is intended to provide a basic understanding of thermal adhesive preloading rather than to quantify the design margins included in the conservative characteristic material values of this study. More sophisticated numerical analyses employing dedicated modelling strategies adapted to cryogenic conditions are being developed in a complementary ongoing study to gain deeper insight into the implications of thermal stresses within the adhesive bondline, particularly in regions known for stress accumulation. Nevertheless, even a simplified linear-elastic analysis demonstrates that reliable material parameters under cryogenic conditions are essential yet remain scarce, underscoring the significance of this study.

3. Test results

The following section presents the test results obtained for Aeropaste 1006, FM 209-1 M, Cryobond 620N, and Cryobond 621. Shear stress – strain curves are plotted for each adhesive. Within these plots, each curve represents the mean of a test series, with the standard deviation indicated as a shaded band. The mean curves are truncated at the failure point of the first specimen in each series. In addition, one table per adhesive is provided, listing the characteristic material properties determined for each series.

3.1. Aeropaste 1006

Figure 10 shows the shear stress-strain curves for the Aeropaste 1006 series. Test results at cryogenic conditions are illustrated in blue (series 1—3). The cryogenic curves exhibit linear behaviour up to the point of stepwise failure. Microscopy images reveal increasingly pronounced fragmentation patterns perpendicular to the load direction with greater bondline thickness. A similar sensitivity to bondline thickness is observed in the shear stress-strain curves. Showing a reduction in linear limit and ultimate load with increasing bondline thickness under cryogenic conditions. Test results at room temperature are illustrated in orange (series 4—6). At room temperature, the adhesive displays a pronounced plastic region after the linear limit. Failure shear strain is also influenced by bondline thickness at room temperature. From RT to CT a substantial decrease in failure shear strain and and increased shear stiffness can be seen in the plot. Microscopy images reveal increasing amounts of defects with thicker bondlines for CT and RT series.

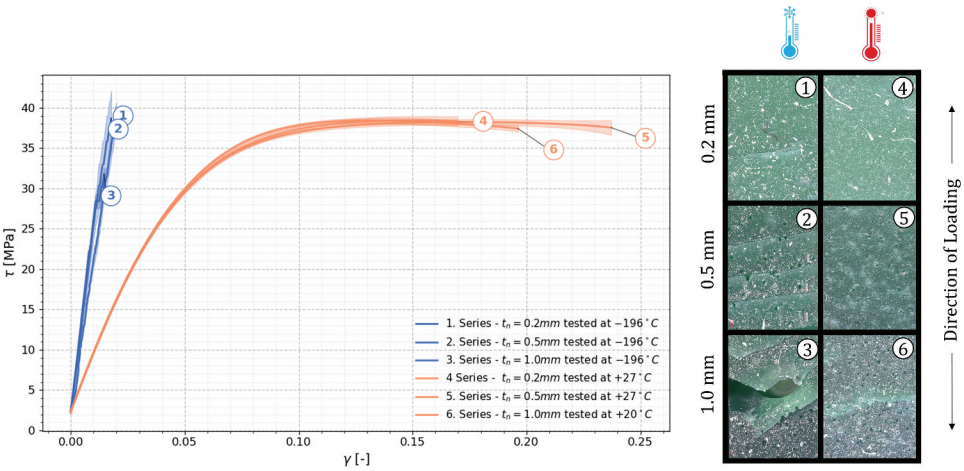

Figure 10. Shear stress - shear strain correlation for six Aeropaste 1006 series and characteristic adhesive fracture surfaces.

Characteristic mechanical values for Aeropaste 1006 at room and cryogenic temperatures with varying bondline thicknesses are summarised in Table 5. At room temperature, the shear modulus remains nearly constant across bondline thicknesses, with reduced variation at higher thicknesses. A similar trend is observed under cryogenic conditions, where thicker bondlines result in more consistent shear modulus values. The linear limit and ultimate load vary only slightly with thickness at room temperature, particularly in terms of stress. However, failure shear strain rises noticeably with thicker bondlines. Under cryogenic conditions, the linear limit shear stress rises significantly compared to room temperature. Ultimate shear strength increases only slightly. In contrast, both the linear limit and failure shear strain are substantially reduced at cryogenic temperatures.

3.2. FM209-1 M

Shear stress-strain curves for the FM209-1 M series are illustrated in Figure 11. At cryogenic temperatures (series 1–3), the adhesive shows predominantly linear behaviour. Microscopy images reveal, more pronounced fragmentation perpendicular to the load direction with increasing thickness. Unlike Aeropaste 1006, no voids are observed. Stiffness remains relatively constant at cryogenic conditions, while failure strength decreases significantly with greater bondline thickness. FM209-1 M exhibits pronounced plastic deformation beyond the linear region at room temperature (series 4–6). The highest failure strains occur at the smallest bondline thickness. In contrast to Aeropaste, the shear stiffness varies significantly across thicknesses at room temperature. Notably, FM209-1 M is typically

Table 5. Characteristic mechanical values for Aeropaste 1006.

Aeropaste 1006						
	Room Temperature (20°C to 27°C)			Cryogenic Temperature (−196°C)		
b_n **[mm]**	0.20	0.50	1.00	0.20	0.50	1.00
G [MPa]	783.13 ± 156.04	751.22 ± 40.02	749.60 ± 14.35	1546.31 ± 971.14	2193.94 ± 307.13	2406.24 ± 254.95
τ_{LL} [MPa]	14.18 ± 1.53	14.00 ± 1.10	14.96 ± 0.66	42.01 ± 4.30	32.45 ± 3.96	30.75 ± 4.15
γ_{LL} [–]	0.017 ± 0.004	0.017 ± 0.002	0.018 ± 0.001	0.021 ± 0.008	0.013 ± 0.002	0.011 ± 0.003
τ_{UL} [MPa]	37.49 ± 0.54	35.86 ± 0.67	35.70 ± 0.59	46.22 ± 3.57	43.41 ± 2.18	36.44 ± 3.32
γ_{UL} [–]	0.216 ± 0.044	0.305 ± 0.034	0.306 ± 0.047	0.026 ± 0.010	0.021 ± 0.004	0.020 ± 0.005
b [μm]	220.64 ± 20.14	488.33 ± 21.46	925.06 ± 15.40	248.23 ± 22.69	493.02 ± 7.03	905.51 ± 20.84
n [—]	7	7	7	4	7	7

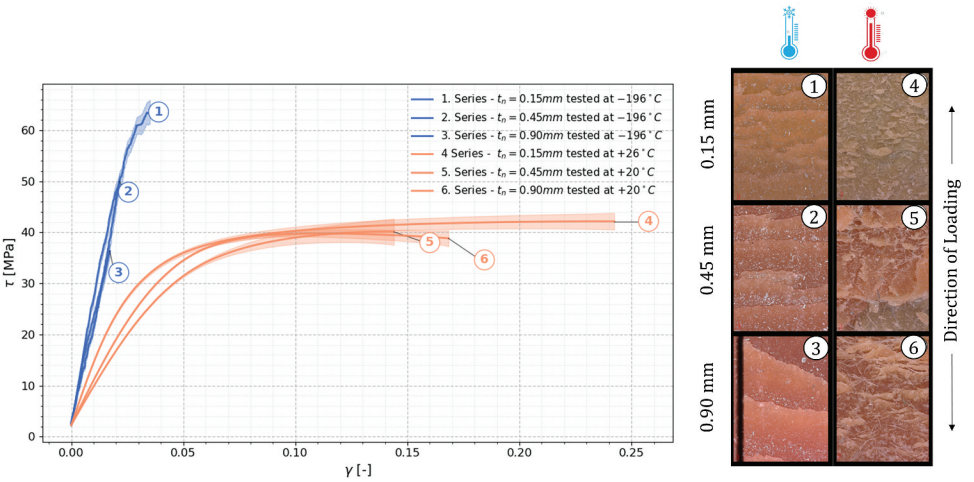

Figure 11. Shear stress - shear strain correlation for six FM209-1M series and characteristic adhesive fracture surfaces.

applied in a single layer, in this study, a stacking of up to six layers was investigated. Characteristic mechanical values for FM209-1 M at room and cryogenic temperatures with varying bondline thicknesses are summarised in Table 6. At cryogenic temperature, the adhesive exhibited the highest ultimate shear strain across the entire test programme at a bondline thickness of 0.15 mm. In this configuration, both the linear limit shear stress and strain were comparatively high. With increasing bondline thickness, a more pronounced stepwise failure was observed, resulting in a significant reduction in the linear-limit shear stress – by approximately a factor of two at 0.45 mm.

3.3. Cryobond 620N

The shear stress – strain behaviour of Cryobond 620N (Figure 12) differs markedly from that of the structural adhesives Aeropaste 1006 and FM209-1 M. A strong sensitivity to bondline thickness is observed at both cryogenic (series 1–3) and room temperature tests (series 4–6). At room temperature, the adhesive exhibits pronounced plasticity for the thinnest bondline, with the linear region ending at approximately 4 MPa. Increasing the bondline thickness results in higher stiffness and strength, and significantly less plastic deformation. For the thickest bondline, the linear limit increases to roughly 10 MPa. At cryogenic temperatures, the adhesive behaves linearly with no discernible plasticity. Despite the high ultimate shear strain observed for the thinnest bondline at room temperature, little of this ductility remains at cryogenic conditions. Both ultimate shear strain and strength decrease with increasing bondline thickness. Unlike structural

Table 6. Characteristic mechanical values for FM209-1 M.

FM209-1M						
	Room Temperature (20°C to 26°C)			Cryogenic Temperature (−196°C)		
b_n[mm]	0.15	0.45	0.90	0.15	0.45	0.90
G [MPa]	1393.57 ± 414.85	773.00 ± 27.39	901.72 ± 36.82	2246.74 ± 981.89	2621.34 ± 546.87	2479.56 ± 603.37
τ_{LL} [MPa]	15.24 ± 3.83	16.52 ± 1.56	17.48 ± 1.08	59.07 ± 2.83	29.18 ± 5.63	20.58 ± 4.00
γ_{LL} [–]	0.011 ± 0.005	0.019 ± 0.002	0.018 ± 0.001	0.027 ± 0.012	0.010 ± 0.002	0.007 ± 0.002
τ_{UL} [MPa]	41.79 ± 1.69	38.57 ± 2.25	35.33 ± 0.58	67.53 ± 3.28	56.22 ± 4.29	48.88 ± 4.74
γ_{UL} [–]	0.542 ± 0.118	0.342 ± 0.053	0.259 ± 0.023	0.055 ± 0.035	0.027 ± 0.005	0.026 ± 0.003
b [μm]	168.18 ± 13.68	475.07 ± 35.67	817.77 ± 25.94	188.02 ± 25.71	438.12 ± 36.32	821.15 ± 33.03
n [—]	7	7	7	6	7	7

adhesives, Cryobond 620N shows no strong tendency for step wise failure. Microscopy did not reveal adhesive fragmentation perpendicular to load direction for specimens tested at cryogenic conditions. The incorporation of air bubbles into the adhesive displayed in Figure 12 could not be avoided, despite close coordination with the manufacturer and repeated production runs. Particularly for the thinnest bondlines, specimens showed a tendency to creep at room temperature. Characteristic mechanical values for Cryobond 620N at room and cryogenic temperatures with varying bondline thicknesses are summarised in Table 7. When comparing the series with the thinnest bondline, Cryobond 620N exhibits a shear modulus comparable to that of FM 209-1 M under cryogenic conditions, despite its flexibility at room temperature.

3.4. Cryobond 621

Unlike the other adhesives investigated, Cryobond 621 is not a pure epoxy system, but contains 70% aluminium fillers by weight. This results in an unusually high stiffness for an adhesive, already evident at room temperature (Figure 13, series 4—6). Upon cooling to cryogenic temperatures, the measured stiffness increases significantly further (Figure 13, series 1—3). Due to the small deformations exhibited by the adhesive, accurate measurement becomes particularly challenging. At room temperature, a transition from linear to plastic behaviour can be observed; however, this transition is not strongly pronounced due to the low ultimate strain. Similarly, only limited failure strains are achieved at cryogenic temperatures. Microscopic analysis of the adhesive fracture surfaces revealed no discernible influence of bondline

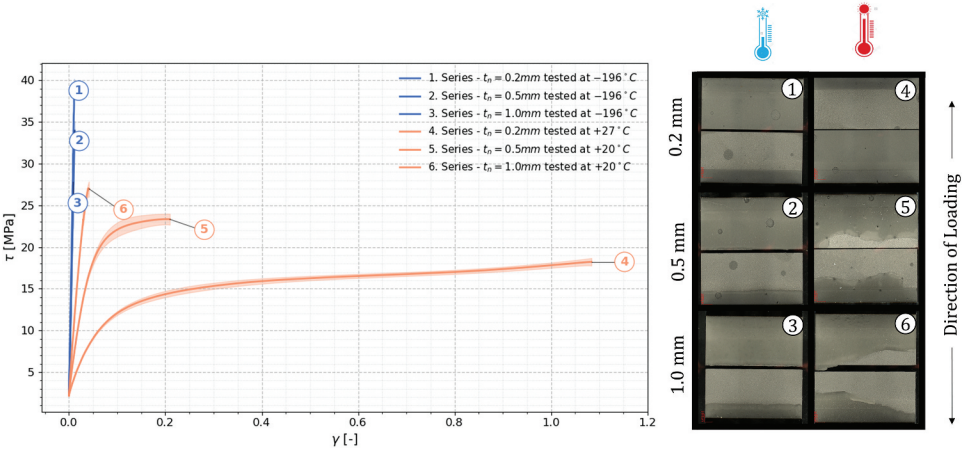

Figure 12. Shear stress - shear strain correlation for six Cryobond 620N series and characteristic joint fracture surfaces.

Table 7. Characteristic mechanical values for Cryobond 620N.

Cryobond 620N						
	Room Temperature (20°C to 27°C)			Cryogenic Temperature (−196°C)		
b_n **[mm]**	0.20	0.50	1.00	0.20	0.50	1.00
G [MPa]	226.53 ± 22.09	509.91 ± 29.47	877.59 ± 25.40	2496.09 ± 845.31	2795.53 ± 791.34	3549.88 ± 740.57
τ_{LL} [MPa]	4.05 ± 0.16	6.74 ± 0.45	10.78 ± 0.62	38.63 ± 7.10	31.00 ± 9.95	33.49 ± 6.49
γ_{LL} [–]	0.009 ± 0.001	0.009 ± 0.001	0.010 ± 0.001	0.011 ± 0.005	0.010 ± 0.003	0.009 ± 0.002
τ_{UL} [MPa]	19.20 ± 1.43	19.41 ± 2.59	27.80 ± 2.10	42.46 ± 1.76	37.50 ± 3.72	34.63 ± 5.29
γ_{UL} [–]	1.251 ± 0.139	0.449 ± 0.167	0.087 ± 0.068	0.011 ± 0.005	0.015 ± 0.003	0.012 ± 0.002
b [μ m]	179.73 ± 15.67	449.45 ± 24.99	921.36 ± 32.38	184.46 ± 8.03	466.35 ± 14.41	926.54 ± 44.95
n [—]	7	5	7	4	4	6

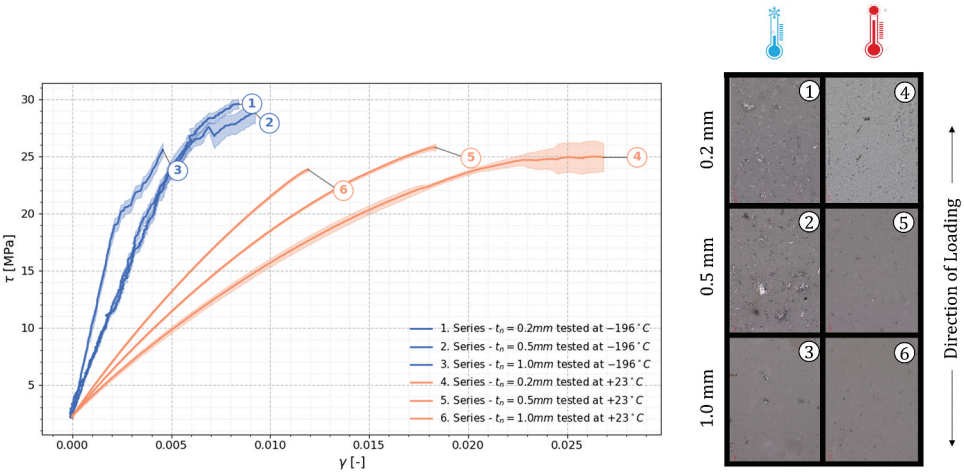

Figure 13. Shear stress - shear strain correlation for six Cryobond 621 series and characteristic joint fracture surfaces.

thickness or temperature on the failure characteristics. Characteristic mechanical values for Crybond 621 at room and cryogenic temperatures with varying bondline thicknesses are summarised in Table 8.

Post-test microscopic inspection revealed adhesive residues on the substrate for adhesives Aeropaste 1006, FM209-1 M, and Cryobond 621, particularly within surface valleys. For Cryobond 620N, its transparency requires further analysis to confirm any residue. All adhesives reached or exceeded the manufacturer-specified failure strengths at room temperature, suggesting that surface pre-treatment was sufficient and no adhesive failure occurred. Under cryogenic conditions, failure appears to initiate near the substrate. While the paste-like systems also fail close to the substrate at room temperature, this transition is especially pronounced for FM 209-1 M.

4. Discussion and conclusion

In this study, a novel experimental method was developed and implemented to characterise the shear stress – strain behaviour of adhesives at cryogenic temperatures down to −196°C. A dedicated test rig and a capacitive extensometer were employed to measure deformation across the bondline. The test procedure was based on ASTM D5656[16] and adapted for cryogenic testing using liquid nitrogen. To ensure high measurement accuracy, and in contrast to the TAST method introduced by Leitwein et al.,[11] displacement was measured in close proximity to the adhesive layer within the overlap area, on both sides of the specimen flanks. In addition, several design measures to avoid specimen misalignment, a series-based manufacturing process, and

Table 8. Characteristic mechanical values for Cryobond 621.

Cryobond 621						
	Room Temperature (23°C)			Cryogenic Temperature (−196°C)		
b_n **[mm]**	0.20	0.50	1.00	0.20	0.50	1.00
G [MPa]	1585.56 ± 137.93	1917.78 ± 73.62	2316.68 ± 290.03	4451.09 ± 1772.67	4977.60 ± 1531.01	7319.90 ± 559.80
τ_{LL} [MPa]	10.95 ± 1.78	13.02 ± 0.74	14.48 ± 1.02	22.81 ± 7.52	23.86 ± 2.02	20.96 ± 1.06
γ_{LL} [–]	0.006 ± 0.001	0.006 ± 0.000	0.006 ± 0.000	0.006 ± 0.004	0.005 ± 0.001	0.002 ± 0.000
τ_{UL} [MPa]	28.67 ± 2.37	26.93 ± 1.19	28.28 ± 2.52	32.89 ± 3.53	31.82 ± 2.70	27.76 ± 3.05
γ_{UL} [–]	0.047 ± 0.010	0.028 ± 0.010	0.018 ± 0.003	0.014 ± 0.005	0.011 ± 0.003	0.006 ± 0.002
b [μ m]	182.64 ± 24.75	355.33 ± 25.06	683.58 ± 143.20	184.64 ± 26.73	437.52 ± 27.07	847.80 ± 154.67
n [—]	7	7	7	6	4	7

microscopic measurement of the overlap area for each specimen were implemented to ensure high reproducibility and comparability of results. To address changes in dielectric properties and parasitic thermal effects within the measurement chain, an additional experiment was carried out using the CryoTAST setup. This experiment established the linear correlation between the measured voltage amplitude signal and the joint displacement, with liquid nitrogen as dielectric medium. The plausibility of this linear correlation was confirmed by comparing the calculated permittivity of liquid nitrogen from the experiment with the reference value reported by Hosking et al.[25]

Motivated by numerous distinct joint problems in the proximity of the CFRP liquid hydrogen tank, the structural adhesives Aeropaste 1006 and FM209-1 M as well as the functional adhesives Cryobond 620N and Cryobond 621 were investigated. To understand the impact of bondline thicknesses tolerances on structural performance, resulting from industrial manufacturing processes, bondline thicknesses ranging from 0.15 mm to 1 mm were investigated. Tests were performed at room and cryogenic temperatures using sets of seven specimens per configuration. Shear stress – strain curves were derived, shear modulus, stress and strain at the linear limit and ultimate load were calculated, including standard deviations. Although structural adhesives demonstrate increased or stable shear strength at cryogenic temperatures (except thick bondlines), they exhibit a reduction in fracture shear strain by more than an order of magnitude, as well as a significant increase in shear stiffness – typically by a factor of 2 to 3. Consequently, strain-based design criteria are recommended. Raffaelli[9] similarly observed a reduction in fracture strain by a factor of 2 to 3 in tensile tests on bone specimens at cryogenic temperatures. Additionally, his results qualitatively indicate a pronounced increase in Young's modulus, as inferred from graphical data, although no absolute values were reported. Within the present study, the performance of structural adhesives was found to be more sensitive to increasing bondline thickness at cryogenic temperatures than at room temperature. This observation must be further examined in the context of the thermo-mechanical stress state within the joint. Considering both strain limitations and bondline thickness, structural adhesives such as Aeropaste 1006 and FM 209-1 M exhibited reliable performance under cryogenic test conditions and static mechanical loading. The observed brittleness of the adhesives at cryogenic conditions, suggests that under cyclic loading conditions, the growth of microcracks may occur, as local stress concentrations within the bondline cannot be relaxed through stress redistribution. This could lead to a reduction in fatigue strength. Therefore, further characterisation under dynamic loading conditions is recommended. While functional adhesives such as Cryobond 620N and Cryobond 621 are not intended for structural applications, their mechanical behaviour nonetheless provides valuable insights for their respective use cases. The initial hypothesis that

aluminium fillers in Cryobond 621 might mitigate thermal expansion mismatch – due to the aluminium adherends – and thereby result in higher failure strains compared to structural adhesives was not supported by the experimental findings. Interestingly, even the functional adhesive Cryobond 620N, which is highly flexible at room temperature when applied as a thin bondline, demonstrated a shear modulus under cryogenic conditions comparable to that of FM 209-1 M. This convergence in mechanical behaviour between a soft epoxy adhesive and a stiff structural epoxy adhesive when subjected to cryogenic conditions was also reported by Raffaelli,[9] based on tensile tests of bone resin specimens at −196°C. Among all test configurations, FM 209-1 M exhibited the highest ultimate shear strain of 0.055 at a bondline thickness of 0.15 mm under cryogenic conditions.

Microscopy analysis of specimens tested under cryogenic conditions revealed predominant fracture patterns perpendicular to the load direction in structural adhesives, particularly with increasing bondline thickness. Bondline fragmentation can be correlated with the observed stepwise joint failure. It is assumed that a key factor influencing this behaviour is the CTE mismatch between the adhesive and the adherends, which induces significant pre-stress during cooling. A linear elastic FE analysis was included in this study to assess the superposition of thermal and mechanical loading of the specimens during cryogenic TAST testing. Based on a basic von Mises stress approach to evaluate the strength utilisation of the adhesive, it can be assumed that the characteristic material values obtained in this study are conservative, as the bearable shear strength of the joint is reduced by the thermal pre-loading. The need for more sophisticated complementary finite element analyses and reliable material data at cryogenic condition was identified.

Measuring strain at cryogenic temperatures remains challenging due to the extremely low deformation at failure – typically around 20 μm — compared to approximately 200 μm at room temperature for TAST specimens. These small deformation values necessitate highly sensitive and precise instrumentation to accurately evaluate joint performance under extreme temperature conditions. This challenge is particularly significant for thin bondlines and for especially stiff adhesives, such as Cryobond 621, which contains 70% aluminium filler. As the adhesive's contribution to the total deformation signal decreases, signal resolution and measurement accuracy deteriorate. This results in greater variability in the derived material properties and more pronounced shaded bands around the mean curves in the shear stress – strain diagrams – a known phenomenon in adhesive testing. For room temperature conditions, Kassapoglou et al.[19] recommend measuring deformation closer to the adhesive layer by reducing the distance between extensometer mounting points or by increasing the bondline thickness in order to increase adhesive deformation portion. The present study includes characteristic values for thicker bondlines

showing a tendency to reduced standard deviation. Further reduction of the distance between measurement points to assess shear strain even closer to the adhesive layer would pose a design challenge, but could be addressed through continued development of the presented extensometer.

Acknowledgments

This research was funded by the German Federal Ministry for Economic Affairs and Climate Action (BMWK) within the framework of the national aviation research programme LuFo VI-2. The project "HYTANK" was supported under grant number 20W2214G. The authors gratefully acknowledge this support.

The authors would also like to thank Syensqo SA for providing the adhesives Aeropaste 1006 and FM 209-1 M, and for their valuable technical input throughout the study.

Furthermore, the authors thank Composite Technology Development, Inc. for their support in developing a manufacturing process for the application of Cryobond 620N and Cryobond 621 dedicated for TAST specimens.

Author contributions

CRediT: **Thomas Gesell:** Conceptualization, Data curation, Formal analysis, Funding acquisition, Investigation, Methodology, Project administration, Resources, Software, Validation, Visualization, Writing – original draft, Writing – review & editing; **Dirk Holzhüter:** Conceptualization, Formal analysis, Methodology, Resources, Supervision; **Jens Kosmann:** Conceptualization, Data curation, Investigation, Methodology, Resources, Supervision; **Martin Johannes Schollerer:** Conceptualization, Methodology, Supervision, Validation; **Patrick Adrian Makiela:** Formal analysis, Investigation, Methodology, Writing – review & editing; **Christian Hühne:** Supervision.

Disclosure statement

No potential conflict of interest was reported by the authors.

Funding

This work was supported by the Federal Ministry for Economic Affairs and Climate Action (BMWK), Germany, under grant number [20W2214G].

ORCID

Thomas Gesell http://orcid.org/0000-0002-1365-4826
Dirk Holzhüter http://orcid.org/0000-0003-1001-2366
Jens Kosmann http://orcid.org/0000-0002-2225-4832
Martin Johannes Schollerer http://orcid.org/0000-0001-7015-9461
Patrick Adrian Makiela http://orcid.org/0009-0000-0975-2733
Christian Hühne http://orcid.org/0000-0002-2218-1223

List of symbols

Symbol	Description	Unit
A	Electrode area	mm^2
b	Bondline thickness	mm
C	Capacitance	F
d	Measured displacement (sensor signal)	mm
d_m	Deformation of adherend	mm
d	Deformation applied using a measurement screw gauge	μm
ε_0	Vacuum permittivity (8.854×10^{-12})	F/m
ε_r	Relative permittivity of dielectric	-
F	Applied force during test	N
G	Shear modulus of the adhesive	MPa
γ	Corrected shear strain	-
I	Alternating current	A
I_0	Amplitude of current	A
K	Integration constant	C
l	Overlap length of adhesive bond	mm
m	Adherend compliance under shear stress state	$\frac{mm}{N}$
m_{RT}	Adherend compliance at cryogenic temperature	$\frac{mm}{N}$
m_{CT}	Adherend compliance at room temperature	$\frac{mm}{N}$
n	Number of specimen	—
ω	Angular frequency of excitation	Hz
p	Bore hole distance on specimen	mm
Q	Electric charge	C
σ	Normal stress	MPa
t	Time	s
τ	Shear stress	MPa
U	Voltage across the capacitor	V
U_0	Demodulated voltage amplitude	V
w	Overlap width of adhesive bond	mm
x, y, z	FE model axes	-

References

[1] Hertz, J. Cryogenic Adhesive Evaluation Study. Convair Division - General Dynamics Corporation, United States Department of Defense - DTIC Defense Technical Information Center, Tech. Rep., 1961. https://apps.dtic.mil/sti/trecms/pdf/AD0273219.pdf .

[2] Hertz, J. An Evaluation of the Mechanical Properties of Adhesives at Cryogenic Temperatures and their Correlation with Molecular Structures. General Dynamics Corporation-Astronautics, United States Department of Defense - DTIC Defense Technical Information Center, Tech. Rep., 1962. https://apps.dtic.mil/sti/tr/pdf/AD0831537.pdf.

[3] Althof, W. Die Festigkeit vonüberlappten Metallklebungen bei tiefen und hohen Temperaturen und nach Temperaturwechseln; Deutsche Forschungsanstalt für Luftund Raumfahrt e.V. Tech. Rep., 1965. https://www.gbv.de/dms/tib-ub-hannover/366779451.pdf.

[4] Gosnell, R. B.; Levine, H. H. Some Effects of Structure on a Polymer's Performance as a Cryogenic Adhesive. *J. Macromol. Sci.: Part A - Chem.* 1969, *3*(7), 1381–1393. issn: 0022-233X. DOI: 10.1080/10601326908051832

[5] Roseland, L. M. Adhesives for Cryogenic Applications. *J. Macromol. Sci. Part B* 1967, *1* (4), 639–650. issn: 0022-2348. DOI: 10.1080/00222346708212354
[6] Williamson, F. R.; Neil, A. O. Cryogenic Adhesives and Sealants: Abstracted Publications. Cryogenics Division of Institute for Basic Standards US National Bureau of Standards, NTRS - NASA Technical Reports Server, Tech. Rep., 1977. https://ntrs.nasa.gov/citations/19770013313.
[7] Goeders, D. C.; Perry, J. L. Adhesive Bonding PEEK/IM-6 Composite for Cryogenic Applications. *36th Int. SAMPE Symp.* 1991, *April*(36), 348–361.
[8] Graf, N. A.; Schieleit, G. F.; Biggs, R. Adhesive Bonding Characterization of Composite Joints for Cryogenic Usage. Lockheed Martin Space Systems Company, NTRS- NASA Technical Reports Server, Tech. Rep., 2000. https://ntrs.nasa.gov/api/citations/20010020380/downloads/20010020380.pdf.
[9] Raffaelli, L. *Thermomechanics of Fibre Reinforced Epoxies for Cryogenic Pressurized Containment*. 2005. https://d-nb.info/985154608/34.
[10] Alberts, S. J.; Doehne, C. J.; Johnson, W. L. Testing Tensile and Shear Epoxy Strength at Cryogenic Temperatures. NASA, NTRS - NASA Technical Reports Server, Tech. Rep. 2017. https://ntrs.nasa.gov/api/citations/20180002104/downloads/20180002104.pdf.
[11] Leitwein, M.; Reiling, K.; Janik, P.; Zauner, C. Cryogenic Adhesive Testing. *ECSSMET* 2021, *16*, 24001.
[12] Leitwein, M.; Reiling, K.; Janik, P. Results of Cryogenic Adhesive Characterization-Part 1: Polymer Characterisation. *ECSSMET* 2023, *17*, 1077–1082.
[13] Glass, D. E. Bonding and Sealing Evaluations for Cryogenic Tanks. NASA Langley Research Center, NTRS - NASA Technical Reports Server, Tech. Rep., 1997. https://ntrs.nasa.gov/api/citations/19970029012/downloads/19970029012.pdf.
[14] Funke, T.; Germer, A.; Haberstro, C.; Mayrhofer, R.; Stipsitz, J. A Test Rig for Analysis of Adhesive Tapes at 4 K Cryogenic Temperature. IOP Conf. Ser.: Mater. Sci. Eng. 2017, *171*, DOI: 10.1088/1757-899X/171/1/012134.
[15] *DIN EN 14869-1:2011-07, Strukturklebstoffe - Bestimmung des Scherverhaltens Struktureller Klebungen - Teil 1: Torsionsprüfverfahren unter Verwendung stumpf verklebter Hohlzylinder (ISO 11003-1:2001, Modifiziert); Deutsche Fassung EN 14869-1:2011*. DOI: 10.31030/1779681.
[16] D14 Committee, *Test Method for Thick-Adherend Metal Lap-Shear Joints for Determination of the Stress-Strain Behavior of Adhesives in Shear by Tension Loading*. DOI: 10.1520/D5656-10R17.
[17] *ISO 11003-2: Adhesives — Determination of Shear Behaviour of Structural Adhesives: Part 2: Tensile Test Method Using Thick Adherends*, 2019.
[18] Volkersen, O. Die Schubkraftverteilung in Leim-, Niet-Und Bolzenverbindungen. *Energ. Tech.* 1953, *5*, 68–54.
[19] Kassapoglou, C.; Adelmann, J. C. KGR-1 Thick Adherend Specimen Evaluation for the Determination of Adhesive Mechanical Properties. *SAMPE Q.* 1992, 19–27.
[20] Kosmann, J.; Völkerink, O.; Schollerer, M.; Holzhüter, D.; Hühne, C. Digital Image Correlation Strain Measurement of Thick Adherend Shear Test Specimen Joined with an epoxy Film Adhesive. *Int. J. Adhes. Adhes.* 2019, *2019*, 32–37. DOI: 10.1016/j.ijadhadh.2019.01.024
[21] Kadioglu, F.; Vaughn, L. F.; Guild, F. J.; Adams, R. D. Use of the Thick Adherend Shear Test for Shear Stress-Strain Measurements of Stiff and Flexible Adhesives. *J. Adhes.* 2002, *78*(78), 355–381. issn: 0021-8464. DOI: 10.1080/00218460211818
[22] Bressler, K.; Martin, R.; Hering, E.; Vogt, A.; Gutekunst, J. *Elektrotechnik Für Maschinenbauer: Grundlagen*; Springer Berlin/Heidelberg, 1997. isbn: 9783662069929.

[23] Reesor, G. E.; Dagg, I. R.; Mohabir, S. The Complex Dielectric Constant of Liquid Nitrogen in the Region 18 to 26 GHz. *Can. J. Phys.* 1975, *53*(23), 2611–2612. DOI: 10.1139/p75-318

[24] Smith, P. A.; Davis, L. E.; Button, T. W.; Alford, N. M. The Dielectric Loss Tangent of Liquid Nitrogen. *Supercond. Sci. Technol.* 1991, *4*(3), 128–129. DOI: 10.1088/0953-2048/4/3/011

[25] Hosking, M. W.; Tonkin, B. A.; Proykova, Y. G.; Hewitt, A.; Alford, N. M.; Button, T. W. The Dielectric Constant of Liquid Nitrogen Over the Frequency Range 0.5 to 10.4 GHz. *Supercond. Sci. Technol.* 1993, *6*(7), 549–552. issn: 0953-2048. DOI: 10.1088/0953-2048/6/7/018

[26] *DIN EN ISO 527-1:2019-12, Kunststoff - Bestimmung Der Zugeigenschaften-Teil 1: Allgemeine Grundsätze (ISO 527-1:2019); Deutsche Fassung EN ISO 527-1:2019*. doi: 10.31030/3059426.

[27] Battelle Memorial Institute. *Metallic Materials Properties Development and Standardization: MMPDS-05*. 2010, isbn: 1–61344–019–7.

[28] Barbero, E. J. *Introduction to Composite Materials Design*; CRC press, 2010. DOI: 10.1201/9781439894132